The Astrophysical Journal Letters, 926:L21 (7pp), 2022 February 20 https://doi.org/10.3847/2041-8213/ac531f

Evidence for Cold-stream to Hot-accretion Transition as Traced by Lyα Emission from Groups and Clusters at $2 < z < 3.3$

E. Daddi[1], R. M. Rich[2], F. Valentino[3,4], S. Jin[3,5], I. Delvecchio[6], D. Liu[7], V. Strazzullo[8], J. Neill[9], R. Gobat[10], A. Finoguenov[11], F. Bournaud[1], D. Elbaz[1], B. S. Kalita[1], D. O'Sullivan[9], and T. Wang[12]
[1] CEA, IRFU, DAp, AIM, Université Paris-Saclay, Université de Paris, Sorbonne Paris Cité, CNRS, F-91191 Gif-sur-Yvette, France
[2] Department of Physics & Astronomy, University of California Los Angeles, 430 Portola Plaza, Los Angeles, CA 90095, USA
[3] Cosmic Dawn Center (DAWN), Denmark
[4] Niels Bohr Institute, University of Copenhagen, Jagtvej 128, DK-2200, Copenhagen N, Denmark
[5] DTU-Space, Technical University of Denmark, Elektrovej 327, DK-2800 Kgs. Lyngby, Denmark
[6] INAF-Osservatorio Astronomico di Brera, via Brera 28, I-20121, Milano, Italy
[7] Max-Planck-Institut fur extraterrestrische Physik (MPE), Giessenbachstr. 1, D-85748 Garching, Germany
[8] Dipartimento di Fisica, Universitá di Trieste, Via Tiepolo 11, I-34143 Trieste, Italy
[9] California Institute of Technology, 1216 East California Boulevard, Pasadena, California 91125, USA
[10] Instituto de Fisica, Pontificia Universidad Catolica de Valparaiso, Casilla, 4059, Valparaiso, Chile
[11] Department of Physics, University of Helsinki, Gustaf Hällströmin katu 2, FI-00014 Helsinki, Finland
[12] School of Astronomy and Space Science, Nanjing University, Nanjing 210093, People's Republic of China
Received 2021 November 23; revised 2022 February 5; accepted 2022 February 7; published 2022 February 21

Abstract

We present Keck Cosmic Web Imager observations of giant Lyα halos surrounding nine galaxy groups and clusters at $2 < z < 3.3$, including five new detections and one upper limit. We find observational evidence for the cold-stream to hot-accretion transition predicted by theory by measuring a decrease in the ratio between the spatially extended Lyα luminosity and the expected baryonic accretion rate (BAR), with increasing elongation above the transition mass ($M_{\rm stream}$). This implies a modulation of the share of BAR that remains cold, diminishing quasi-linearly (logarithmic slope of 0.97 ± 0.19, 5σ significance) with the halo to $M_{\rm stream}$ mass ratio. The integrated star formation rates (SFRs) and active galactic nucleus (AGN) bolometric luminosities display a potentially consistent decrease, albeit significant only at 2.6σ and 1.3σ, respectively. The higher scatter in these tracers suggests the Lyα emission might be mostly a direct product of cold accretion in these structures rather than indirect, mediated by outflows and photoionization from SFR and AGNs; this is also supported by energetics considerations. Below $M_{\rm stream}$ (cold-stream regime), we measure $L_{\rm Ly\alpha}/{\rm BAR} = 10^{40.51\pm0.16}$ erg s^{-1} $M_\odot^{-1}$ yr, consistent with predictions, and ${\rm SFR/BAR} = 10^{-0.54\pm0.23}$: on average, 30^{+20}_{-10}% of the cold streams go into stars. Above $M_{\rm stream}$ (hot-accretion regime), $L_{\rm Ly\alpha}$ is set by $M_{\rm stream}$ (within 0.2 dex scatter in our sample), independent of the halo mass but rising 10-fold from $z = 2$ to 3.

Unified Astronomy Thesaurus concepts: Galaxy evolution (594); Galaxy accretion (575)

1. Introduction

It has long been understood from theory that galaxies in dark matter halos below $M_{\rm shock} \approx 10^{12} M_\odot$ are fed by cold accretion, delivering gas ready to form stars (White & Frenk 1991; Birnboim & Dekel 2003; Kereš et al. 2005; Dekel & Birnboim 2006, DB06 hereafter), driving high SFRs in distant galaxies (e.g., Genel et al. 2008). Above $M_{\rm shock}$, cooling times are longer than dynamical times, and shocks can efficiently heat incoming baryons.

However, numerical simulations and analytical work from Dekel & Birnboim (2006) first showed that cold accretion continues to penetrate at high redshifts in the form of cold streams even above $M_{\rm shock}$, in massive halos located at the intersection of multiple and dense filaments, narrower than the halos they accrete onto. This is crucial for feeding even more massive galaxies (e.g., Daddi et al. 2007) residing in massive halos at high redshifts (e.g., Béthermin et al. 2014). Subsequent numerical and analytical modeling developed this theory with respect to stream stability (Nelson et al. 2015; Mandelker et al. 2019), multiphase properties (Cornuault et al. 2018), additional inner-halo cooling (Zinger et al. 2018; Mandelker et al. 2019, 2020), and angular momentum transfer to galaxies (Danovich et al. 2015). This cold-stream mode should be effective up to an evolving halo mass $M_{\rm stream}(z)$, expected to be of the order of $10^{12.5} M_\odot$ at $z = 2$ and growing to $10^{13.5} M_\odot$ at $z = 3$ (DB06), and rapidly diluted and disappearing at even higher masses.

Observational confirmation is still lacking for cold streams and for evidence that the $M_{\rm stream}$ transition affects gas accretion observables. Cold streams are predicted to be best detectable via their collision-powered Lyα emission (Dijkstra & Loeb 2009; Goerdt et al. 2010; Rosdahl & Blaizot 2012). However, deep Lyα observations of distant massive groups and clusters are still scarce. In this Letter, we present results from our ongoing KCWI survey targeting nine massive galaxy structures at $2 < z < 3.5$, providing Lyα-based evidence of the predicted dilution of cold streams across $M_{\rm stream}$. We adopt concordance cosmology (0.3; 0.7; 70) and a Chabrier IMF.

2. Data and Measurements

We describe our sample selection and characterization of some important aspects of the structures (Table 1). A complete

Table 1
Galaxy Groups and Clusters Used in This Work

ID	R.A.	Decl.	z (1)	$\log(M_{\rm DM})$ ($M_\odot$) (2)	$\log(L_{\rm Ly\alpha})$ (ergs s^{-1}) (3)	log(SFR) ($M_\odot$ yr^{-1})	$\log(L_{\rm AGN})$ (ergs s^{-1}) (4)	log(BAR) ($M_\odot$ yr^{-1})	$\log(\frac{M_{\rm stream}}{M_{\rm DM}})$	$T_{\rm int}$ h	SB corr dex
XLSSC 122	02:17:44.19	−03:45:31.5	1.98	14.2	<43.0	<2.3	<45.3	4.4	−1.8	0.75	⋯
Cl-1449	14:49:14.05	08:56:24.6	1.992	13.8	43.5	2.8	45.5	3.9	−1.4	3.6	⋯
FVX-LAB	09:58:42.32	02:00:39.3	2.194	13.0	43.6	2.1	45.3	3.1	−0.4	1.0	⋯
Cl-1001	10:00:57.18	02:20:08.4	2.501	13.9	43.6	3.2	45.0*	4.2	−0.9	5.0	⋯
CC-0958	09:58:52.97	01:58:02.8	2.515	13.6	43.9	2.3	<44.6*	3.9	−0.6	2.0	⋯
RO-1001	10:01:23.06	02:20:04.9	2.915	13.6	44.1	3.1	44.9*	4.0	−0.1	8.5	⋯
RO-0959	09:59:59.48	02:34:41.7	3.096	12.8	44.0	3.2	45.1	3.1	0.9	1.5	0.07
SXDS-N-LAB1	02:18:21.31	-04:42:33.1	3.109	13.1	44.0	2.2	<44.9*	3.4	0.6	1.0	0.08
RO-0958	09:58:19.79	02:36:10.1	3.295	12.9	43.3	3.2	45.5*	3.2	1.0	1.25	0.18

Note. (1) The redshift is from the luminosity-weighted Lyα emission for all but XLSSC 122 where it is from optical spectroscopy (Willis et al. 2020). (2) We use M_{200}; for XLSSC 122 we converted M_{500} into M_{200} with a 1.7× scaling. (3) SB corrections are already applied. (4) * indicates values inferred from Lyα point-source components (or lack there-of);

description of the fields will be given elsewhere (E. Daddi et al. 2022, in preparation).

2.1. Sample Selection

The nine structures include several that are already well known: Cl-1449 (e.g., Valentino et al. 2016), Cl-1001 (Wang et al. 2016), RO-1001 (Daddi et al. 2021 D21 hereafter), CC-0958 (Strazzullo et al. 2015), and XLSSC 122 (Mantz et al. 2018). We present here two new radio overdensities (RO-0959 and RO-0958), selected following Daddi et al. (2017). We also include two Lyα blobs, SXDS-N-LAB1 (Matsuda et al. 2011; Subaru narrowband imaging) and FVX-LAB (from our own narrowband imaging in COSMOS).

2.2. KCWI Observations and Redshift Identification

All the targets were observed with KCWI during observing runs in 2018 January and 2019 February. The data reduction and analysis, including diffuse Lyα identification and characterization via adaptive smoothing over a 3σ threshold, follow D21's work for RO-1001. We detect giant Lyα nebulae in all structures (>100 kpc; Figure 1), except the most massive/evolved XLSSC 122 where we determine a conservative 3σ upper limit over 1000 km s^{-1} and 200 arcsec^2. We confirm known nebulae: the Lyα luminosity of Cl-1449 agrees with that of Valentino et al. (2016), while SXDS-N-LAB1 is 2.4× brighter than that in Matsuda et al. (2011), consistent with its emission being partly redshifted out of their narrowband filter.

Figure 1 shows three-band color images of eight structures newly observed in Lyα (see D21 for RO-1001). This includes a new giant Lyα halo discovery inside Cl-1001. The photometric redshifts of RO-0958 and RO-0959 were confirmed by Lyα detections, implying $z = 3.29$ and 3.09, respectively. These have been subsequently confirmed with ALMA from the detection of multiple CO lines (E. Daddi et al. 2022, in preparation). CC-0958 had a tentative $z \sim 2.18$ (Strazzullo et al. 2015) but KCWI revealed its giant Lyα halo at $z = 2.51$, still consistent with its photometric redshift.

The Lyα luminosities in Table 1 are integrated above a redshift-dependent surface brightness (SB) of $2 \times 10^{-18} \times [(1 + 2.78)/(1 + z)]^4$ erg s^{-1} cm^{-2} arcsec^{-2} to account for SB dimming. We need (small) positive luminosity corrections only for the three $z > 3$ structures (Table 1), where the observed SB limits are shallower than this threshold. Corrections were estimated using the other five profiles as a guide, with uncertainties <0.05 dex.

The Lyα luminosities in Table 1 refer to the extended, diffuse emission only: For all structures, we identified Lyα components arising from galaxies (generally active galactic nuclei (AGNs); see below) and removed their contribution, modeling them with the PSF as all remain unresolved at our resolution (typically 0.″6–0.″8). This correction is ∼15% for FVX-LAB and RO-0958, and much smaller elsewhere.

2.3. Estimates of Host Halo Masses, SFRs, and AGN Content

Host halo-mass ($M_{\rm DM}$) estimates were already presented elsewhere for several structures (XLSSC 122, Cl-1449, Cl-1001, and RO-1001), where derivations based on their stellar-mass (M^*) content were confirmed via X-ray luminosities and in two cases from the Sunyaev–Zel'dovich effect (SZ; XLSSC 122 in Mantz et al. 2018; Cl-1449 in Gobat et al. 2019). For the other structures, we derive estimates from the M^* following D21. We consider spectroscopic members and those with consistent photometric redshifts (Muzzin et al. 2013; Laigle et al. 2016; Mehta et al. 2018), spatially coincident within the area of the structure, as gauged by the Lyα halo and self-consistently with the implied virial radius. The integrated M^* above the completeness limit for the redshift is corrected to total using the mass functions in Muzzin et al. (2013) and converted to $M_{\rm DM}$ using van der Burg et al. (2014). For CC-0958 we find a marginal 2.4σ detection in Chandra, fully consistent with the M^*-based estimate. For the higher-mass systems with $M_{\rm DM} \gtrsim 4 \times 10^{13} M_\odot$, we estimate $M_{\rm DM}$ uncertainties at the level of 0.2 dex or better, at least in relative terms, by comparing the M^*, X-ray, and SZ derivations.

For the lower-mass systems ($M_{\rm DM} \lesssim 1 \times 10^{13} M_\odot$) we check that consistent estimates are derived using the brightest group galaxy, applying the relations in van der Burg et al. (2014) and Behroozi et al. (2013). We expect these estimates to be uncertain at the 0.3–0.4 dex level (e.g., Looser et al. 2021).

Integrated bolometric IR luminosities were presented elsewhere for Cl-1449, Cl-1001, and RO-1001 (refs in Sect. 2.1). We derived them for the other structures using Herschel PACS and SPIRE (plus other submillimeter) observations, as described in D21 for RO-1001. Their uncertainties are small, below 0.2 dex. We set a conservative 3σ upper limit from

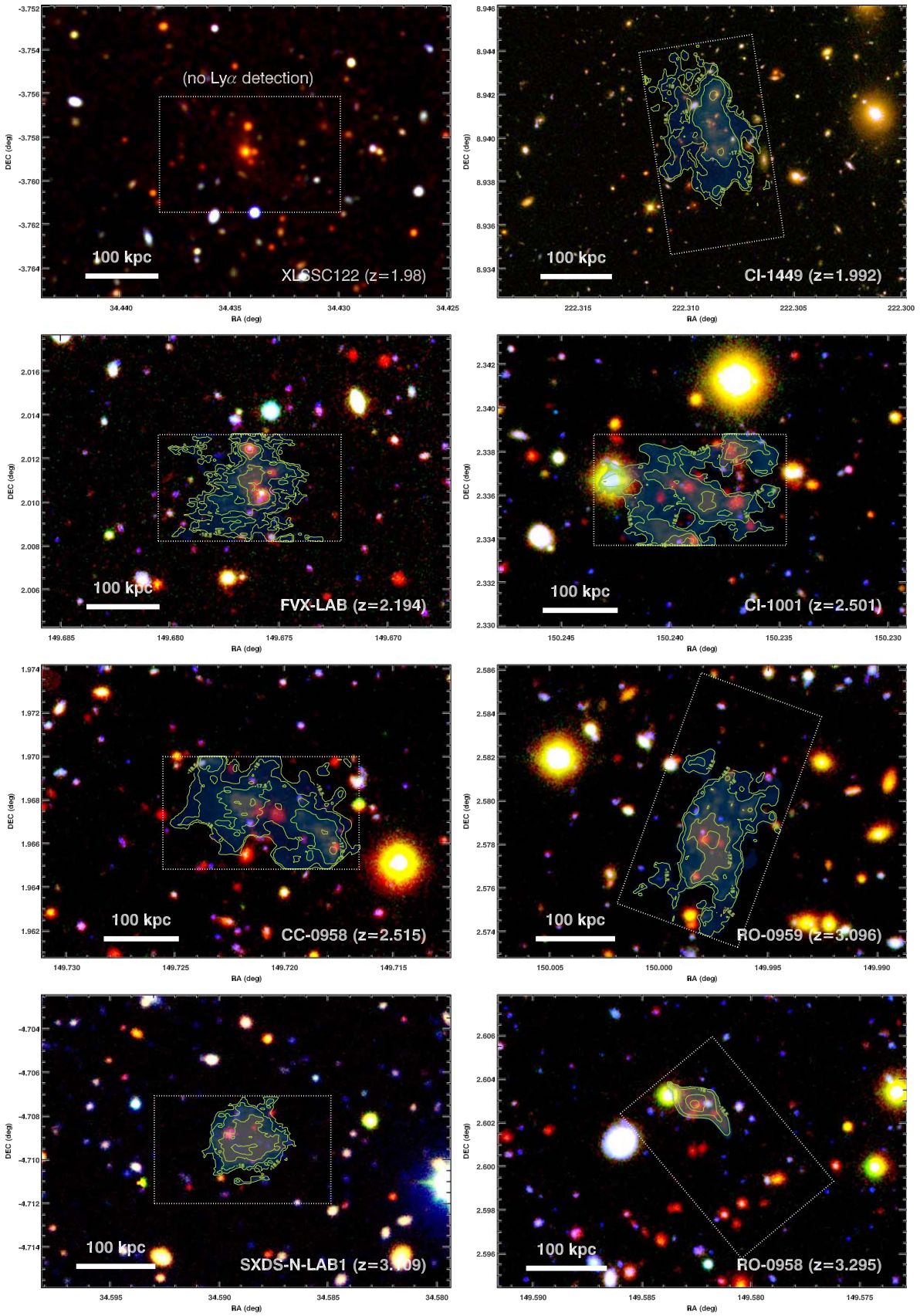

Figure 1. Color images of spectroscopically confirmed targets for which KCWI Lyα observations are first presented here (BzK for most, or close variations; north is up and east is left). Cl-1449 is from HST; the rest is ground-based. See D21 for a similar RO-1001 image. The blue soft layer shows Lyα emission, with contours displayed in log steps from –18.5 to –17.5 erg s^{-1} arcsec^{-2} as labeled. The dotted lines show the KCWI field. The orientation of the RO fields was chosen to maximize overlap with the radio detections.

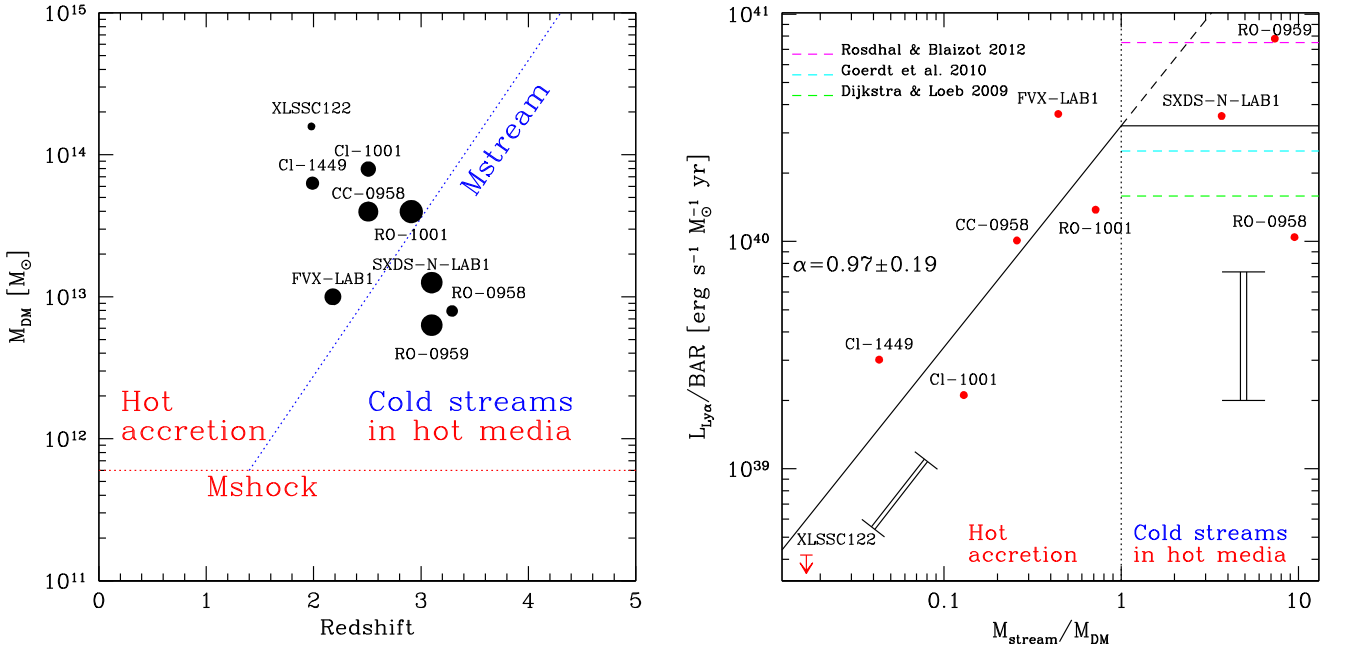

Figure 2. (Left) Our sample in the DB06 diagram. Symbol sizes are proportional to $L_{\mathrm{Ly}\alpha}$ (Table 1). The blue diagonal line defines M_{stream} (Equation (2)). (Right) The ratio of the extended Lyα luminosity in the structures is plotted vs. the M_{stream} to halo-mass ratio. The relation in Equation (4) is fitted (solid black line). Typical uncertainties are shown: 0.2 dex along the slope above M_{stream}, 0.3 dex along the y-axis below M_{stream}. Predictions for $M_{\mathrm{DM}} < M_{\mathrm{stream}}$ (cold-stream regime) are shown (colored dashed lines).

nondetections in XLSSC 122. We convert IR luminosities into SFRs following Daddi et al. (2007).

We used ancillary Chandra X-ray catalogs (Civano et al. 2016; Marchesi et al. 2016; Mantz et al. 2018) and SED decomposition (e.g., Jin et al. 2018) to search for known AGNs within the expected virial radius of the structures. AGNs are found for Cl-1449, FVX-LAB, and RO-0959. Their bolometric luminosities ($L_{\mathrm{bol,AGN}}$) were either calculated from the mid-IR torus emission from SED fitting (e.g., Jin et al. 2018) or its upper limit. If available and more constraining, intrinsic X-ray luminosities scaled to bolometric (Lusso et al. 2012) were used instead. For these AGNs, we find coincident point-like Lyα emission with a ratio of $\log L_{\mathrm{AGN,bol}}/L_{\mathrm{AGN,Ly}\alpha} \sim 2.9 \pm 0.2$, consistent with Sloan QSOs for their narrow Lyα component (Vanden Berk et al. 2001; Norman et al. 2002). We use this relation to estimate $L_{\mathrm{AGN,bol}}$ from Lyα point-like galaxy components in RO-1001, Cl-1001, and RO-0958, and upper limits for the remainder. For RO-1001 this implies $L_{\mathrm{AGN,bol}} \sim 10^{44.9}$ erg s^{-1} (in Galaxy-C), consistent with D21.

The average AGN/SFR ratio in our structures is consistent with the cosmic average (Mullaney et al. 2012; Delvecchio et al. 2019), excluding strong relative enhancements of either quantity.

3. Results

We calculate the total halo BAR using Equation 5 from Goerdt et al. (2010) (using the equivalent formulations from Genel et al. 2008 or Dekel et al. 2013 would not affect our results):

$$\mathrm{BAR} \simeq 137\left(\frac{M_{\mathrm{DM}}}{10^{12}M_{\odot}}\right)^{1.15}\left(\frac{(1+z)}{(1+3)}\right)^{2.25} M_{\odot}\mathrm{yr}^{-1}, \quad (1)$$

and from Figure 7 in DB06 we use $M_{\mathrm{shock}} = 6 \times 10^{11} M_{\odot}$ and approximate M_{stream} as

$$\log M_{\mathrm{stream}} \simeq \log M_{\mathrm{shock}} + 1.11 \times (z - 1.4). \quad (2)$$

Figure 2, left, shows the location of our sample in the DB06 diagram, spreading across the M_{stream} boundary. Figure 2, right, shows the ratio of $L_{\mathrm{Ly}\alpha}$ to BAR for our sample as a function of the $M_{\mathrm{stream}}/M_{\mathrm{DM}}$ ratio.

According to theory, cold streams should feed galaxies and halos for $M_{\mathrm{DM}} < M_{\mathrm{stream}}$ at $z > 1.4$, where cold accretion is equal to total accretion as in Equation (1), while for $M_{\mathrm{DM}} > M_{\mathrm{stream}}$ one can expect a smooth transition where an increasingly lower fraction of accretion will be cold (DB06). We define

$$\mathrm{BAR}_{\mathrm{cold}} \simeq \begin{cases} \mathrm{BAR}\left(\dfrac{M_{\mathrm{stream}}}{M_{\mathrm{DM}}}\right)^{\alpha} & M_{\mathrm{DM}} > M_{\mathrm{stream}} \\ \mathrm{BAR} & M_{\mathrm{DM}} \lesssim M_{\mathrm{stream}} \end{cases}. \quad (3)$$

We model observables that are expected to be dependent on the availability of cold fuel as

$$L_{\mathrm{Ly}\alpha} = C_{\mathrm{Ly}\alpha} \times \mathrm{BAR}_{\mathrm{cold}}, \quad (4)$$

where $C_{\mathrm{Ly}\alpha}$ is a constant and the slope from Equation (3) becomes $\alpha_{\mathrm{Ly}\alpha}$. Similar relations are considered for integrated SFRs and $L_{\mathrm{bol,AGN}}$, with their modulation slopes α_{SFR} and α_{AGN}, and constants C_{SFR} and C_{AGN}.

Figure 2, right, shows a behavior quite consistent with Equation (4). A linear fit to the data attempting to constrain its two free parameters returns $\alpha_{\mathrm{Ly}\alpha} = 0.97 \pm 0.19$ and $\log C_{\mathrm{Ly}\alpha} = 40.51 \pm 0.16$ with a scatter of 0.30 dex. Paired bootstrap (with replacements) implies similar uncertainties. The modulation of decreasing Lyα luminosity to accretion ratio $\alpha_{\mathrm{Ly}\alpha}$, when the halo mass is larger than M_{stream}, is hence detected at 5σ. $C_{\mathrm{Ly}\alpha}$ is consistent within a factor of 2 with

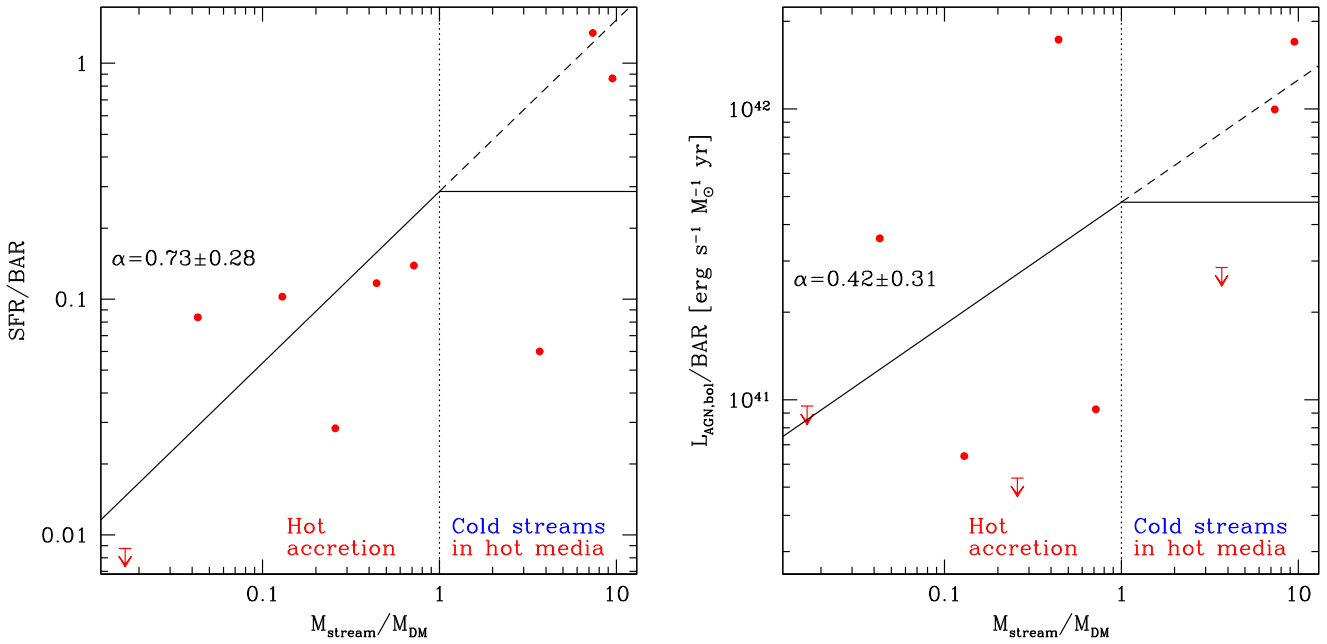

Figure 3. As in Figure 2, right, but for SFR (left) and AGNs (right). Notice the especially poor correlation with $L_{\rm AGN}$/BAR.

model predictions (Dijkstra & Loeb 2009; Goerdt et al. 2010; Rosdahl & Blaizot 2012; Figure 2-right), where roughly 1% of the gravitational energy goes into Lyα. Note that we are assuming the flattening in the right side of Figure 2, right, not measuring it. However, if we were to extrapolate the linear fit in Figure 2, right, above $M_{\rm stream}/M_{\rm DM} > 1$ (dashed line), the observed $L_{\rm Ly\alpha}$ there would deviate by 4.8σ in one case (RO-0958) and 1.5σ in the other two, with all three weaker than predicted by the extrapolation. This is unlikely to happen by chance, supporting the assumed flattening.

For the ratio SFR/BAR, we find a consistent behavior (Figure 3, left), but less significant (2.6σ): $\alpha_{\rm SFR} = 0.78 \pm 0.28$ and $\log C_{\rm SFR} = -0.54 \pm 0.23$, with a 0.45 dex scatter. Below $M_{\rm stream}$ (cold-stream regime), some 20%–50% of the cold accretion goes into SFR, on average (with a scatter of 3×). These fractions appear reasonable (Dekel et al. 2009), given that some reduced efficiency seems inevitable as not all the cold gas will be rapidly consumed. Above $M_{\rm stream}$ (hot regime), SFR/BAR in $z \sim 2$–2.5 structures is higher by 3×–10× than predicted by Behroozi et al. (2013).

For AGNs we find only a 1.3σ hint of a trend (Figure 3-right), still consistent with a slope of ∼1 within 2σ: $\alpha_{\rm AGN} = 0.42 \pm 0.31$ and $\log C_{\rm AGN} = 41.70 \pm 0.26$, with an rms of 0.51 dex.

4. Discussion

4.1. Reliability of the Detection

From our admittedly small and inhomogeneous sample, we find observational evidence in support of the cold-stream to hot-accretion transition predicted by theory. It is crucial to assess its validity. Figure 2 contains the relations among various quantities, including estimates based on observables ($L_{\rm Ly\alpha}$ and $M_{\rm DM}$) and calculated from theory ($M_{\rm stream}$ and BAR; Equations (1) and (2)) that depend in turn on z and $M_{\rm DM}$. Redshift and Lyα luminosity errors are negligible with respect to the scatter observed in the fit. Hence, $M_{\rm DM}$ is the most critical quantity in our analysis. For $M_{\rm DM} < M_{\rm stream}$ (cold-stream regime), $L_{\rm Ly\alpha}$/BAR is set to constant ($C_{\rm Ly\alpha}$; Equation (1)), because cold BAR equals total BAR. The uncertainty in $C_{\rm Ly\alpha}$ is 0.16 dex, consistent with $M_{\rm DM}$ error propagation ($0.3/\sqrt{5}$ dex), indirectly confirming the error estimates. In the hot regime ($M_{\rm DM} > M_{\rm stream}$), the three structures with the highest $M_{\rm DM}/M_{\rm stream}$ are the ones with the best halo-mass determination, estimated from X-ray and SZ measurements. By themselves, they set a slope of $\alpha_{\rm Ly\alpha} \approx 1$ with respect to the rest of the sample. This simplifies, to first order, to Equations (1) and 2 to $L_{\rm Ly\alpha} \propto M_{\rm stream}$, and we find indeed $L_{\rm Ly\alpha}/M_{\rm stream} = 10^{30.75\pm0.20}$ erg s^{-1} $M_\odot^{-1}$ with just a 0.20 dex scatter, implying that $L_{\rm Ly\alpha}$ grows by 1 dex over $\Delta z = 1$, similarly to $M_{\rm stream}$. Hence, in the hot regime (and for $\alpha \approx 1$) a precise determination of $M_{\rm DM}$ is not required to measure α. Our conclusions are thus not critically dependent on $M_{\rm DM}$ uncertainties.

4.2. Physical Interpretation

It is important to question whether the correlation shown in Figure 2, right, arises from a direct link between cold accretion rate and Lyα luminosity (Figure 4, right), or an indirect one, with accretion regulating SFR and $L_{\rm bol,AGN}$ that in turn determine Lyα emission, e.g., by photoionization and subsequent recombinations (see D21 for more discussions). If the latter, it would be difficult to explain how Lyα can define a tighter relation to accretion than SFR and AGN if Lyα was a byproduct of these quantities. D21 already suggested cold accretion as the main source of Lyα powering in RO-1001, rather than AGN or SFR. However, it is worth reconsidering the matter here with a larger sample of structures.

Starting from SFRs, basically in all cases, the most highly star-forming members are heavily dust extinguished (Figure 1); their contribution to Lyα photoionization from UV-unattenuated SFR appears negligible, as in D21.

AGN photoionization should be more carefully considered as a plausible source for powering Lyα, at least in some of our structures. We estimate Lyα photoionization rates from $L_{\rm bol,AGN}$ (measurements or upper limits) using bolometric

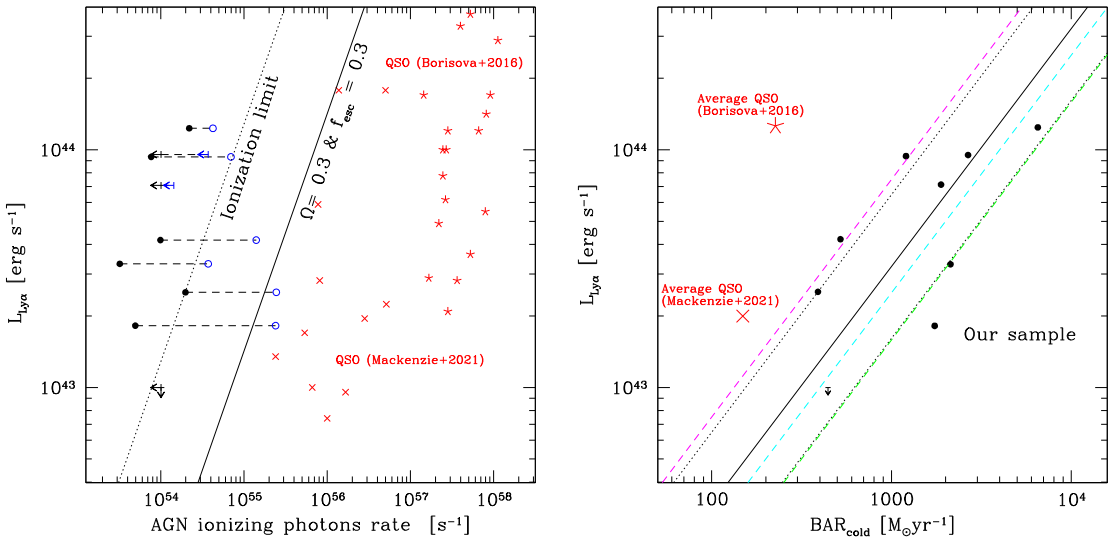

Figure 4. (Left) The Lyα luminosity vs. the AGN ionizing photon rates for our sample (black points estimated from the ultraviolet luminosity, blue empty points connected by dashed lines are computed from $L_{\rm bol,AGN}$; see the text). The diagonal lines show the Lyα luminosity that AGNs can ionize: theoretical maximum (dotted) and (solid) assuming a 30% escape fraction (Smith et al. 2020) and an opening angle $\Omega = 30\%$ (Simpson 2005). (Right) The Lyα luminosity vs. the cold accretion rate, as resulting from Equation (3). The solid (dotted) line(s) shows the average linear trend (1σ range). The colored dashed lines are models as in Figure 2-, right (Dijkstra & Loeb 2009; Goerdt et al. 2010; Rosdahl & Blaizot 2012). In both panels, QSO-selected Lyα nebulae are shown, individually in the left panel and averaged in the right panel where the QSOs' average hosting $M_{\rm DM}$, hence BAR, are estimated from Eftekharzadeh et al. (2015).

corrections to the ultraviolet (Trakhtenbrot & Netzer 2012) and the Type 1 QSO average spectrum (Lusso et al. 2015). Figure 4, left, shows that the maximum theoretical AGN ionizing radiation is potentially sufficient to power $L_{\rm Ly\alpha}$ only in four of the nine structures. When considering that at these luminosities the Type 1 opening angle is expected to be $\sim$30% (Simpson 2005; possibly too large for our sample where no unobscured AGN is found from the nine structures, Figure 4) and the Lyman continuum escape is $\sim$30% (Smith et al. 2020; also likely an overestimate given that our AGNs are embedded in high dust optical depths based on ALMA detections), only two structures remain marginally viable to be fully AGN photoionized, ignoring further geometrical effects (Valentino et al. 2016).

Our sample is compared in Figure 4 to Lyα nebulae selected around QSOs from Borisova et al. (2016) and Mackenzie et al. (2021). Their Lyα photoionization rates to $L_{\rm Ly\alpha}$ ratios are one to two orders of magnitude larger, on average, with respect to structures in our sample (Figure 4, left). Also, QSOs are significantly overluminous in their average ratio of Lyα emission to cold accretion rates (Figure 4, right). It is thus possible that our structures' Lyα powering is not coming from photoionization, as for the QSOs.

Although these figures show scatter, and the impact of AGNs (and SFR) might vary and be somewhat larger in individual cases, the favored scenario is currently that their contribution is not dominant to Lyα in massive groups and clusters at $2 < z < 3.3$, at least for those in the cold-stream regime.

In the hot regime, if $\alpha_{\rm SFR}$ and $\alpha_{\rm AGN}$ were to be truly flatter than $\alpha_{\rm Ly\alpha}$, this could suggest the contributions from SFR and AGN to Lyα being increasingly important with growing $M_{\rm DM}/M_{\rm stream}$. Such behavior would be physically motivated by the longer timescales required for SFR quenching and residual gas consumption (of order 100–300 Myr; AGNs just reflecting the SFR with increased stochasticity), with respect to Lyα from accretion that is likely a more instantaneous measure. Determining $\alpha_{\rm SFR}$ ($\alpha_{\rm AGN}$) to sufficient precision, e.g., 5σ, would require larger samples of $\sim$50 ($\sim$200) massive groups and clusters.

4.3. Predicting Lyα Luminosities for Dark Matter Halos

The good fit of Equations (3)–(4) to Figure 2, right, is encouraging in terms of using Lyα to trace accretion, hence ultimately halo masses, e.g., for unveiling dark matter halo locations in protoclusters. Using the measured $C_{\rm Ly\alpha}$, Equations (1)–(4) can be rewritten in the cold-stream regime as

$$\log L_{\rm Ly\alpha}/{\rm erg\ s^{-1}} \sim 43.6 + \log \frac{M_{\rm DM}}{10^{13} M_\odot} + 2.25 \log \frac{1+z}{1+3}, \quad (5)$$

depending (quasi)linearly on $M_{\rm DM}$. $L_{\rm Ly\alpha}$ can increase only until $M_{\rm DM}$ reaches $M_{\rm stream}$. From that point on, in the hot-accretion regime, $L_{\rm Ly\alpha}$ is roughly constant depending only on redshift, regardless of how large $M_{\rm DM}$ reaches (because $\alpha_{\rm Ly\alpha} \sim 1$). The data (although using only six objects) allow us to fix the numerical parameters as

$$L_{\rm Ly\alpha}/{\rm erg\ s^{-1}} \sim 10^{42.6} \left(\frac{1+z}{1+1.4}\right)^{\sim 7} \quad \text{for } M_{\rm DM} > M_{\rm stream}, \quad (6)$$

implying that the typical Lyα nebula in the hot regime (and saturation level for the cold regime) is $\approx 10^{43.3}$ erg s^{-1} at $z = 2$ and $\approx 10^{44}$ erg s^{-1} at $z = 3$. The exponent recovered is lower than that fixed by theory (Equations (1) and (2)), perhaps suggesting a less steep $M_{\rm stream}$ redshift dependence (see the discussion in the appendices to Dekel et al. 2009). These predictions can be tested with larger samples.

In conclusion, we report widespread giant Lyα nebulae in massive groups/clusters at $2 < z < 3.3$, with the only non-detection being the most evolved cluster. The Lyα luminosity is a smoothly decreasing fraction of the total baryonic accretion onto these massive halos for the range where models predict

that cold streams should progressively cease feeding halos, thus supporting these models.

We thank Dawn Erb for sharing calibrations, Sebastiano Cantalupo for his CubEx code and discussions, and the referee for a constructive report. R.M.R. acknowledges GO-15910.002 from the Space Telescope Science Institute. Data were obtained at the W. M. Keck Observatory, operated as a scientific partnership among the California Institute of Technology, the University of California, and the National Aeronautics and Space Administration, made possible by the generous financial support of the W. M. Keck Foundation. The authors also acknowledge the indigenous Hawaiian community and are grateful for the opportunity to collect data from the summit of Maunakea.

ORCID iDs

E. Daddi https://orcid.org/0000-0002-3331-9590
R. M. Rich https://orcid.org/0000-0003-0427-8387
I. Delvecchio https://orcid.org/0000-0001-8706-2252
D. Liu https://orcid.org/0000-0001-9773-7479
F. Bournaud https://orcid.org/0000-0002-5743-0250
D. Elbaz https://orcid.org/0000-0002-7631-647X
B. S. Kalita https://orcid.org/0000-0001-9215-7053
T. Wang https://orcid.org/0000-0002-2504-2421

References

Civano, F., Marchesi, S., Comastri, A., et al. 2016, ApJ, 819, 62
Behroozi, P. S., Wechsler, R. H., & Conroy, C. 2013, ApJ, 770, 57
Béthermin, M., Kilbinger, M., Daddi, E., et al. 2014, A&A, 567, A103
Birnboim, Y., & Dekel, A. 2003, MNRAS, 345, 349
Borisova, E., Cantalupo, S., Lilly, S. J., et al. 2016, ApJ, 831, 39
Cornuault, N., Lehnert, M. -D., Boulanger, F., & Guillard, P. 2018, A&A, 610, A75
Daddi, E., Dickinson, M., Morrison, G., et al. 2007, ApJ, 670, 156
Daddi, E., Jin, S., Strazzullo, V., et al. 2017, ApJL, 846, L31
Daddi, E., Valentino, F., Rich, R. M., et al. 2021, A&A, 649, A78
Danovich, M., Dekel, A., Hahn, O., et al. 2015, MNRAS, 449, 2087
Dekel, A., & Birnboim, Y. 2006, MNRAS, 368, 2
Dekel, A., Birnboim, Y., Engel, G., et al. 2009, Natur, 457, 451
Dekel, A., Zolotov, A., Tweed, D., et al. 2013, MNRAS, 435, 999
Delvecchio, I., Daddi, E., Shankar, F., et al. 2019, ApJL, 885, L36
Dijkstra, M., & Loeb, A. 2009, MNRAS, 400, 1109
Eftekharzadeh, S., Myers, A. D., White, M., et al. 2015, MNRAS, 453, 2779
Genel, S., Genzel, R., Bouché, N., et al. 2008, ApJ, 688, 789
Gobat, R., Daddi, E., Coogan, R. T., et al. 2019, A&A, 629, A104
Goerdt, T., Dekel, A., Sternberg, A., et al. 2010, MNRAS, 407, 613
Jin, S., Daddi, E., Liu, D., et al. 2018, ApJ, 864, 56
Kereš, D., Katz, N., Weinberg, D. H., & Davé, R. 2005, MNRAS, 363, 2
Laigle, C., McCracken, H. J., Ilbert, O., et al. 2016, ApJS, 224, 24
Looser, T. J., Lilly, S. J., Sin, L. P. T., et al. 2021, MNRAS, 504, 3029
Lusso, E., Comastri, A., Simmons, B. -D., et al. 2012, MNRAS, 425, 623
Lusso, E., Worseck, G., Hennawi, J. F., et al. 2015, MNRAS, 449, 4204
Mackenzie, R., Pezzulli, G., Cantalupo, S., et al. 2021, MNRAS, 502, 494
Mandelker, N., Nagai, D., Aung, H., et al. 2019, MNRAS, 484, 1100
Mandelker, N., Nagai, D., Aung, H., et al. 2020, MNRAS, 494, 2641
Mantz, A. B., Abdulla, Z., Allen, S. W., et al. 2018, A&A, 620, A2
Marchesi, S., Civano, F., Elvis, M., et al. 2016, ApJ, 817, 34
Matsuda, Y., Yamada, T., Hayashino, T., et al. 2011, MNRAS, 410, L13
Mehta, V., Scarlata, C., Capak, P., et al. 2018, ApJS, 235, 36
Mullaney, J. R., Daddi, E., Béthermin, M., et al. 2012, ApJL, 753, L30
Muzzin, A., Marchesini, D., Stefanon, P., et al. 2013, ApJSS, 206, 8
Nelson, D., Genel, S., Vogelsberger, L., et al. 2015, MNRAS, 448, 59
Norman, C., Hasinger, G., Giacconi, R., et al. 2002, ApJ, 571, 218
Rosdahl, J., & Blaizot, J. 2012, MNRAS, 423, 344
Simpson, C. 2005, MNRAS, 360, 565
Smith, B. M., Windhorst, R. A., Cohen, S. H., et al. 2020, ApJ, 897, 41
Strazzullo, V., Daddi, E., Gobat, R., et al. 2015, A&A, 576, L6
Trakhtenbrot, B., & Netzer, H. 2012, MNRAS, 427, 3081
Valentino, F., Daddi, E., Finoguenov, A., et al. 2016, ApJ, 829, 53
van der Burg, R. F. J., Muzzin, A., Hoekstra, H., et al. 2014, A&A, 561, A79
Vanden Berk, D. E., Richards, G. T., Bauer, A., et al. 2001, AJ, 122, 549
Wang, T., Elbaz, D., Daddi, E., et al. 2016, ApJ, 828, 56
White, S. D. M., & Frenk, C. S. 1991, ApJ, 379, 52
Willis, J. P., Canning, R. E. A., Noordeh, E. S., et al. 2020, Natur, 577, 39
Zinger, E., Dekel, A., Birnboim, Y., et al. 2018, MNRAS, 476, 56